YALE
PEABODY
MUSEUM

P.O. BOX 208118 | NEW HAVEN CT 06520-8118 USA | PEABODY.YALE. EDU

JOURNAL OF MARINE RESEARCH

The *Journal of Marine Research,* one of the oldest journals in American marine science, published important peer-reviewed original research on a broad array of topics in physical, biological, and chemical oceanography vital to the academic oceanographic community in the long and rich tradition of the Sears Foundation for Marine Research at Yale University.

An archive of all issues from 1937 to 2021 (Volume 1–79) are available through EliScholar, a digital platform for scholarly publishing provided by Yale University Library at https://elischolar.library.yale.edu/.

Requests for permission to clear rights for use of this content should be directed to the authors, their estates, or other representatives. The *Journal of Marine Research* has no contact information beyond the affiliations listed in the published articles. We ask that you provide attribution to the *Journal of Marine Research*.

Yale University provides access to these materials for educational and research purposes only. Copyright or other proprietary rights to content contained in this document may be held by individuals or entities other than, or in addition to, Yale University. You are solely responsible for determining the ownership of the copyright, and for obtaining permission for your intended use. Yale University makes no warranty that your distribution, reproduction, or other use of these materials will not infringe the rights of third parties.

This work is licensed under a Creative Commons Attribution-NonCommercial-ShareAlike 4.0 International License.
https://creativecommons.org/licenses/by-nc-sa/4.0/

Secular variability in the baroclinic structure of the interior North Pacific from 1950-1970

by Warren B. White[1]

ABSTRACT

Recently White (1975) found significant year to year changes in the baroclinic transport of the Subtropical Gyre in the North Pacific. To determine the spatial variability in the general circulation associated with this change in bulk transport, the baroclinic potential energy (BPE) in the mid-latitude interior from 20-50N, 145E-130W is mapped (using the methods of optimum interpolation) onto a regular 5 degree latitude/10 degree longitude grid each year from 1950-1970. Subsequently empirical orthogonal function analysis yields two principal spatial patterns of BPE variability that account for nearly 70% of the total interannual variance. The first empirical pattern (accounting for 47% of the interannual variance) shows the intensities of the Subtropical and Subarctic Gyres in the western North Pacific to have fluctuated directly out of phase with one another, with a correlation time scale of approximately 3 years. This was because maximum variability in BPE lay in the transition region between these two gyre systems. The second empirical pattern (accounting for 20% of the interannual variance) shows the intensity of the Subtropical Gyre in the western North Pacific to have fluctuated with a correlation time scale of approximately 1½ years, with little change recorded in the Subarctic Gyre. This was because the variability maxima lay in the centers of the Subtropical Gyre in the western North Pacific. This had the effect of the Subtropical Gyre expanding and contracting in the meridional direction with the changes in the transport.

The range of variability in the Kuroshio extension accounted for by these two empirical patterns was ±50% of the climatological mean baroclinic transport. This was much larger than might be expected; however, when compared with the time sequences of other indices of the component currents around the Subtropical Gyre (e.g., White, 1975; Nitani, 1975; Wyrtki, 1974) qualitative agreement is found, indicating that the component current systems of the Subtropical Gyre tend to have fluctuated in unison with one another. On the other hand, the transport of the Subtropical Gyre tends to have fluctuated out of phase with that of the Subarctic Gyre, such that fluctuations in the bulk transport of the North Pacific Current were much less than that of the component currents.

1. Introduction

It has for many years been within the capability of oceanographers to investigate theoretically the year-to-year, large-scale variability in the ocean general circulation.

1. Scripps Institution of Oceanography, University of California, San Diego, California, 92132, U.S.A.

The investigation into short-term global climate depends upon this kind of effort. However, work along these lines has not proceeded as far as it could, primarily for lack of the oceanographic observations which are needed to confirm the model results. Lately, this situation has begun to change.

Recently, it has become possible to investigate directly the large-scale variability in the oceanic general circulation: first, because more data from new sources are becoming available to monitor the changes in general circulation; second, because more powerful statistical techniques are becoming available to extract meaningful variability from existing oceanographic data sets. As an example of the first change, Wyrtki (1974) has constructed a network of new and existing sea level stations over the equatorial North Pacific that are utilized to monitor the year to year variability in surface speed of the equatorial current systems. An example of the second is the utilization of optimum interpolation methods by McWilliams (1976) to extract the potential vorticity balance from the MODE I hydrographic data obtained in the North Atlantic. It is expected that the utilization of these latter satistical techniques on the historical hydrographic data for the North Pacific will lead to a new understanding about how the large-scale general circulation in the North Pacific changes in time and space.

In the North Pacific, studies within the last few years have begun to substantiate the existence of large-scale, secular, changes within the general circulation of the Subtropical Gyre. In the tropical North Pacific, Wyrtki (1974) has found the surface currents of both the North Equatorial Current and the North Equatorial Countercurrent to fluctuate $\pm 25\%$ about the mean, with a time scale (i.e., quarter period) of approximately 2 years. In the mid-latitude region, Nitani (1975) and White (1975) have found the western boundary current and the interior currents (respectively) of the Subtropical Gyre to fluctuate approximately $\pm 25\%$ about the mean with a time scale similar to that found by Wyrtki (1974). These studies indicate that the general circulation of the Subtropical Gyre of the North Pacific contains significant large-scale, secular, variability. It is the purpose of this study to link these previous efforts in a study of how the baroclinic structure of the Subtropical Gyre in the North Pacific fluctuated in time and space between 1950 and 1970.

The basic analysis in this investigation is the mapping of the interannual changes in the baroclinic structure of the interior North Pacific from 1950-1970. The variable representing the bulk measure of the baroclinic structure is the baroclinic potential energy (BPE), chosen for study because gradients of this quantity are related to the baroclinic transport per unit width (0/500 db). Therefore, maps of this variable yield the pattern of the general circulation in the upper ocean.

The method of mapping the BPE from the individual hydrographic stations follows from the optimum interpolation methods developed by Gandin (1963). The interpolation techniques are discussed at length due to particular biasing and aliasing problems that arise from the irregular space-time distribution of the individual BPE

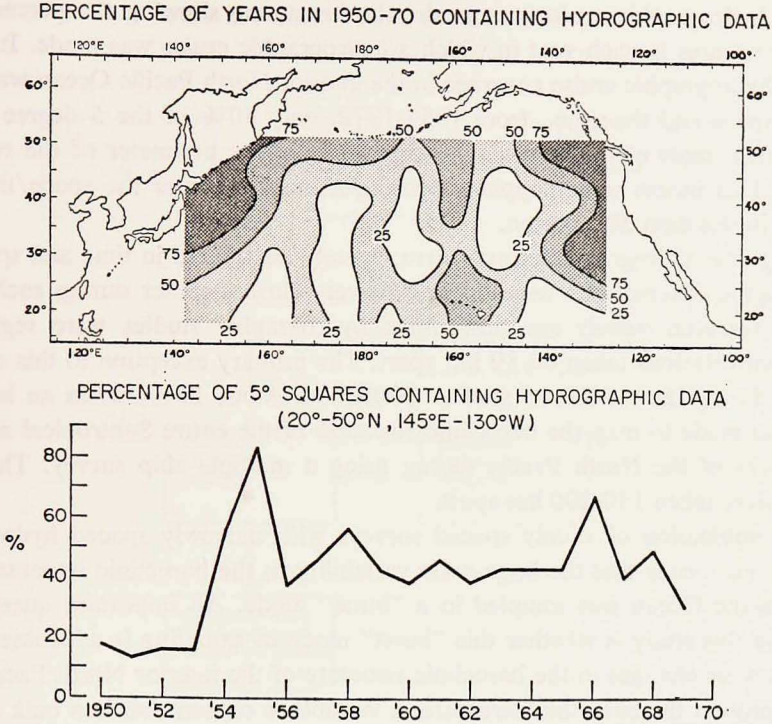

Figure 1. Summary of the hydrographic data distribution in time and space.

observations. The uniform grid is chosen to be 5 degrees latitude, 10 degrees longitude, 1 year, extending over the geographical region from 20N to 50N and from 145E to 130W, and the time period 1950-70.

To synthesize the information contained in these maps, the method of empirical orthogonal function analysis is employed. This method produces characteristic spatial patterns of variability that account for a major portion of the total interannual variance contained in the yearly maps. These patterns are discussed in some detail.

2. Oceanographic data

The data used in this study are derived from the NODC hydrographic file for the North Pacific Ocean. The time period extends from 1950-1970; the region covers the interior North Pacific Ocean from 20 to 50N and from 145E to 130W, away from the eastern and western boundaries. Only observations that extend to 500 m depth or deeper are used.

First, consider the distribution of the hydrographic cruises. In Figure 1 are two panels, the upper one showing the percentage of years in each 5 degree square in

which a hydrographic cruise was made, the lower one showing the percentage of 5 degree squares in each year in which a hydrographic cruise was made. It is clear that the hydrographic cruise coverage in the interior North Pacific Ocean was sparse in both space and time; i.e., from 1954-1970, only 50% of the 5 degree squares were visited, most of these within 10 degrees from the perimeter of the region of interest. This means that mapping procedures must consider the space/time bias inherent in this data distribution.

Though the hydrographic cruises were sparsely distributed in time and space, the hydrographic observations were taken relatively close together during each cruise. Because research vessels are slow, most hydrographic studies were regional in nature, with stations taken 60-80 km apart. The primary exception to this occurred in 1955 during the NORPAC studies (NORPAC Atlas, 1960) when an initial attempt was made to map the baroclinic structure of the entire Subtropical and Subarctic gyres of the North Pacific Ocean using a multiple ship survey. There, the stations were taken 150-200 km apart.

The combination of widely spaced surveys with narrowly spaced hydrographic observations means that the large-scale variability in the baroclinic structure of the North Pacific Ocean was sampled in a "burst" mode. An important question addressed in this study is whether this "burst" mode of sampling is adequate to map the large-scale changes in the baroclinic structure of the interior North Pacific.

To represent the baroclinic structure, a variable is chosen that is a bulk measure of the density structure in the upper ocean. It is the baroclinic potential energy, defined as:

$$\mathrm{BPE} = \rho_0 \, g \int_{500\mathrm{m}}^{0} \int_{500\mathrm{m}}^{z} \alpha \, dz \, dz \,, \tag{2.1}$$

where α is the specific volume, ρ_0 is the average density of the column, and z is the depth from the sea surface. The horizontal distribution of BPE yields information on the baroclinic volume transport of the upper ocean. Through the geostrophic relationship, the gradient of BPE is associated with the baroclinic volume transport per unit width ($\vec{M}$), where

$$\vec{M} = \frac{\hat{k} \times \nabla_H \, \mathrm{BPE}}{f \rho_0} \tag{2.2}$$

In the above expression, f is the Coriolis parameter, ρ_0 is the mean density of the column and $\hat{k}$ is the vertical unit vector. Because (2.2) is analogous to the definition of the vertically integrated velocity streamfunction, isopleths of BPE on a horizontal map, taking into account the β-effect, delineate paths along which the vertically integrated baroclinic flow travels.

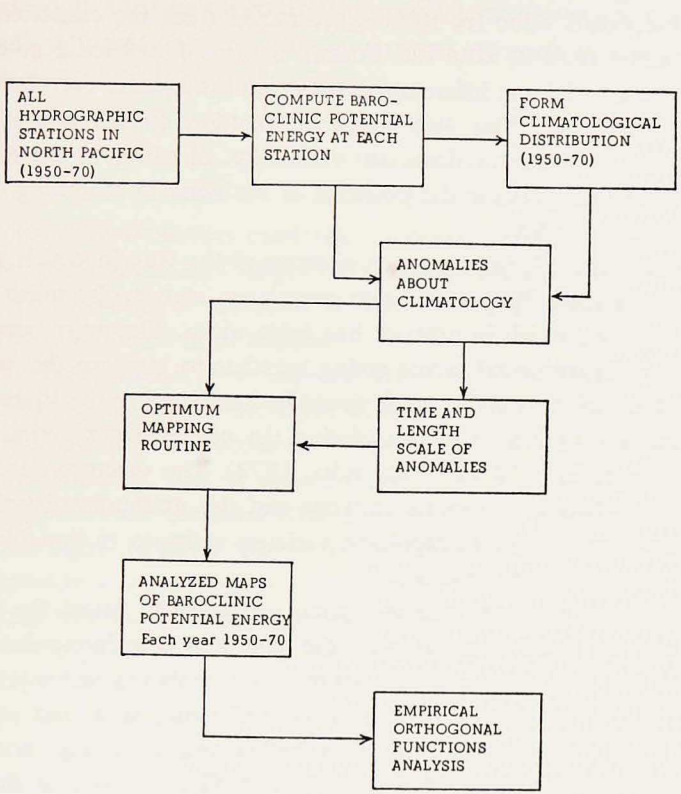

Figure 2. Schematic diagram of the methodology used in this study.

3. Method of optimum interpolation

A description is given of the mapping procedures for BPE, outlined in Figure 2. First, the time and space scales that the "burst" mode of sampling can detect are determined. This is accomplished using auto-covariance techniques, with the added result that the grid needed to resolve this space/time variability is defined. The data are then interpolated to this regular grid. The method of interpolation is called "optimum interpolation," developed by Gandin (1963), and is particularly useful in generating time sequences of maps from data that are irregularly distributed in time and space. The method first interpolates the observed data to some fixed grid consistent with the resolution of the dominant signal; then computer contour programs produce horizontal maps of the signal.

The procedure for determining the space/time scales that can be detected is as follows. First, the BPE at each hydrographic station is computed. Second, the climatological mean distribution of BPE for the 21 year period of interest is com-

puted on a 1 degree latitude/longitude grid, as is the variance about the mean. Third, each individual value for BPE is subtracted from the climatological mean, forming a residual (RBPE) data set. Fourth, a three-dimensional auto-covariance matrix is computed, yielding information upon the space/time correlation scales of the dominant variability. This also yields information on the proper space/time resolution needed to detect the dominant variability. In addition, the sub-grid noise level can be estimated, yielding the potential of the noise in inhibiting the mapping of the large-scale variability.

Before proceeding, it is important to understand the way in which the signal to noise ratio is estimated. Within the auto-covariance matrix, the noise is found in the zero lag position, which in practice has finite width. The noise consists of sub-grid aliasing and instrumental errors acting together to increase the covariance at zero lag (i.e., the variance) above what would be attributed to the signal alone. The signal variance is estimated by extrapolating the covariance function away from zero lag into the origin (Alaka and Elvander, 1972). The variance due to the noise is the difference between the sample variance and this extrapolated estimate of the signal variance. The ratio of extrapolated variance estimate to that of the noise is the square of the signal to noise ratio.

Having established both the grid resolution necessary to detect the signal in the RBPE field and the signal to noise ratio, the next step is to interpolate the station RBPE data to this grid, done with the optimum interpolation techniques developed by Gandin (1963). This method is derived by minimizing, in a least squares sense, the expected RMS interpolation error. This method produces maps not only of the desired variable, but also of its RMS error. The RMS error governs the size of the contour interval within the variable maps.

This interpolation method has obvious advantages over others that have appeared in the literature. First, compared to manual contouring of data, it removes the subjective bias. Second, compared with low-pass filtering, it reduces the spatial and temporal bias that this procedure often entails. This is particularly important in dealing with the present data set, where the "burst" mode of sampling has an enormous potential for spatial and temporal bias. Third, compared with polynomial fit procedures, it constructs a map that is consistent with the natural time and length scales of variability, not those arbitrarily imposed. Moreover, the method optimizes the interpolation and produces error maps, neither of which these other methods do.

To understand better the development of this interpolation procedure, consider the following brief description; for a rigorous treatment see Gandin (1963). The interpolation estimate $\hat{F}$ at the grid node (x, y, t) is determined according to:

$$\hat{F}(x, y, t) = \sum_{i=1}^{N} \alpha_i F_i (x, y, t) , \tag{3.1}$$

where F_i represents the individual observations surrounding the grid node location,

and α_i the weighting coefficient associated with each observation. It is the weighting coefficients that must be determined, found by minimizing in a least squares sense the RMS difference between the interpolated value, $\hat{F}$, at the grid node and the true value there. This leads to the relation:

$$\sum_{j=1}^{N} \mu_{ij}\, \alpha_j + \lambda^2\, \alpha_i = \mu_{0i}\,, \tag{3.2}$$

where μ_{ij} is the autocorrelation coefficient between points i and j and λ^{-1} is the signal to noise ratio. In (3.2), i ranges from 1 to N, resulting in a set of N linear equations to be solved for N unknown α_i by matrix inversion. This matrix inversion is repeated at each grid node location.

In (3.2), the computation of α_i depends upon the knowledge of the space/time auto-correlation matrix, μ, and the signal to noise ratio, λ^{-1}. Within the interpolation scheme the role of μ is to constrain the interpolation, consistent with the dominant scales of variability, and to reduce spatial and temporal bias (i.e., the non-random relation between the local data distribution and the statistical structure). The role of the signal to noise ratio is to reduce the weight, α_i, given to the surrounding observations depending upon how large λ^2 is in (3.2).

To undertand how the RMS interpolation error, E, behaves, consider its makeup:

$$E = \sigma\,[1 - \sum_{i=1}^{N} \mu_{0i}\, \alpha_i]^{\frac{1}{2}} \tag{3.3}$$

The RMS interpolation error depends upon two factors; the relative distribution of the observations about the grid node through μ_{0i}, and the variance, σ^2, at the grid node, the latter containing variance due to the signal alone; the noise enters this calculation through α_i. In the absence of observations, the largest error that can exist is the standard deviation of the field; as observations are added, E is reduced as α_i takes on positive values.

4. Time and length scales

The climatological mean field of baroclinic potential energy from 1950-1970 is examined, as well as its variance. From the mean field the station BPE values are subtracted, forming residual BPE (RBPE) values at each station location. These residuals are then used to compute the auto-covariance matrix discussed in the previous section. From inspection of this covariance matrix, the dominant time and length scales of variability in BPE are determined, as well as the signal to noise ratio.

The climatological mean map of BPE over the North Pacific, computed on a 1 degree grid from hydrographic data taken over the time period from 1950-1970, is

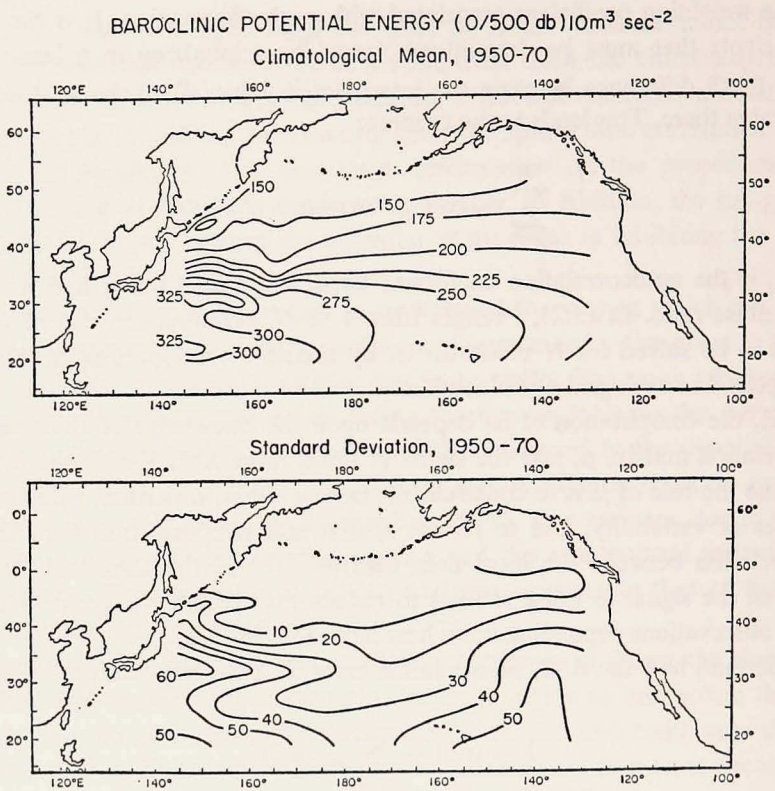

Figure 3. The horizontal distribution of the climatological mean and variance (standard deviation is shown) of BPE (0/500 db) from 1950-1970.

shown in Figure 3. Because isopleths of BPE are directly proportional to those of the vertically integrated velocity streamfunction, the average baroclinic flow over the upper 500 m can be inferred. This traces out the climatological mean general circulation for the North Pacific Current and major portions of both the Subarctic and Subtropical Gyres. West of 165E, the relatively intense nature of the Kuroshio and Oyashio extensions is in contrast to the eastward monotonically decreasing magnitude of the North Pacific current; also the western Subtropical Gyre is composed of two secondary gyres, one at 30N and the other at 20N, separated by an eastward flowing countercurrent near 25N, the latter first identified by Yoshida and Kidokoro (1967) as the Subtropical Countercurrent. This latter feature is also found in the more recent renditions of the annual mean surface geopotential anomaly maps of both Wyrtki (1975) and Reid and Arthur (1975). The Subarctic Gyre is manifested by a trough in BPE running northeast from a minimum centered at 43N, 150E, again in basic agreement with the surface geopotential anomaly maps of Wyrtki (1975) and Reid and Arthur (1975).

The mean baroclinic transport for the Subtropical Gyre is computed by taking

the difference in BPE [integrating (2.2)] from the center of the gyre at 30N, 150E to the edge of the gyre (defined as the 175 line in Figure 3). The resulting transport is found to be approximately 20 Sv (0/500 db), while that for the Subarctic gyre is computed to be approximately 5 Sv. Both of these measurements are consistent with previous efforts to evaluate them (e.g., White, 1975; and Reid, 1973, respectively).

Also displayed in Figure 3 is the RMS of the individual RBPE, representing the total standard deviation of the individual BPE values about the 1 degree climatological mean statistic. This sample statistic combines the signal variance of the expected large-scale variability with the noise variance due both to instrumental error and to mesoscale and seasonal fluctuations. The largest variability exists near the boundaries of the interior ocean, with minimum variability near the center. In the western interior ocean, the largest variability exists along the axis of the Kuroshio/Oyashio extension, with its distribution north and south of it appearing remarkably like the gradients of the mean general circulation. Wyrtki (1975) finds a similar distribution in the standard deviation of surface geopotential anomaly for the western North Pacific, suggesting that in this region of the North Pacific the variance and mean circulation are linked. In the eastern interior ocean, the variability does not appear to have been related to the gradients in the general circulation; rather, it seems to have been largely latitude dependent, decreasing toward the north. There is the possibility that the relative maximum near 20N, 140W is an artifact due to the lack of data near that location (Fig. 1). In fact, Wyrtki (1975) refuses to contour the standard deviation of the surface geopotential anomaly in this region; however, data do exist in this region and they have been contoured in the present study. On the other hand, the relative minimum in the central ocean is not an artifact of the data distribution, since not only does this compare with the earlier results of Wyrtki (1975), but it can be seen (Fig. 1) that relatively good data coverage existed all along the 160W meridian.

The RBPE values are next used to compute the auto-covariance matrix in time and space. From the work of Wyrtki (1967), Bernstein and White (1974), and Dantzler (1976), the variability associated with mesoscale baroclinic eddies in the North Pacific (with scales of 150 km and 1 month) can be expected to contaminate the resolution of the large-scale mean currents, particularly in the western portion of the North Pacific. Similarly, from the work by Wyrtki (1975), Meyers (1975), and White (1977), the variability associated with the seasonal cycle of the major current systems in the North Pacific (with scales of 3 months) can be expected to contaminate the resolution of the annual mean currents. Therefore, by choosing lag sizes in the covariance matrix of 5 degrees latitude, 5 degrees longitude, and 1 year in time, the large-scale variability can be detected while relegating the mesoscale eddy activity and seasonal fluctuations to the first lag position where it manifests itself strictly as subgrid noise.

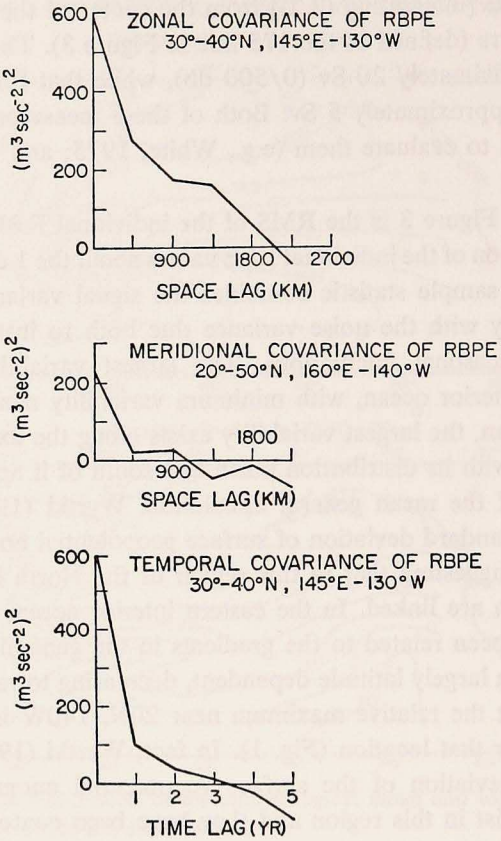

Figure 4. Spatial and temporal covariance estimates for the interior North Pacific.

The three orthogonal traces (i.e., along time, zonal space, and meridional space) of the covariance matrix of RBPE are shown in Figure 4, where the dominant zonal space scale was ~ 2,000 km, the dominant meridional space scale was ~ 1,000 km and the dominant time scale was ~ 3 years. The space scales are not only consistent with those of seasonal-mean, sea surface temperatures in the mid-latitude North Pacific (Namias, 1972), but also with the subsurface temperature variability in the main thermocline of the mid-latitude North Pacific (White and Bernstein, 1977). The time scales are consistent with those of the subsurface temperature features at ocean weather stations P (50N, 145W), N (30N, 140W) and V (34N, 164E) (White and Walker, 1974) in the North Pacific and with the inter-annual variability in near surface baroclinic flow at various locations about the Subtropical Gyre (Wyrtki, 1974; White, 1975; and Nitani, 1975).

In an attempt to establish that these statistics are stationary in space, the RBPE data set is divided into two parts, one east of 180, and the other west. This follows

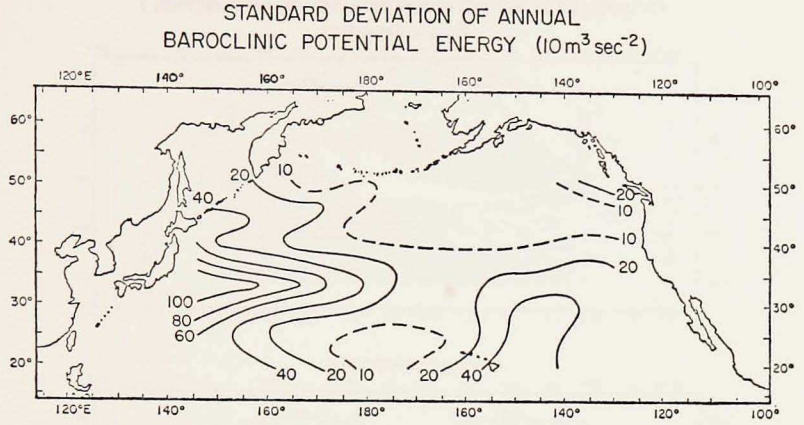

Figure 5. The horizontal distribution of large-scale variance (standard deviation is shown) of BPE, calculated as the RMS of the IRBPE.

from the variance distribution in Figure 3, where the variance in the western mid-latitude North Pacific was much larger than in the eastern portion. However, the auto-covariance matrix from both subregions showed no discernable difference in either time or space scales. This indicates that the large scale variability contained in the RBPE field had structural statistics that were essentially independent of longitude. No test was made of statistical stationarity in time or in latitude.

As discussed earlier, the auto-covariance matrix also yields an estimate of the signal to noise ratio. The noise is the subgrid variance, thought to be composed primarily of baroclinic eddy activity and seasonal fluctuations; the signal is the variance of the large scale features in the absence of this subgrid noise. It was found that, on the average, $\lambda^{-1} = 1.0$ at a particular location indicating that the noise is comparable to the signal.

On the basis of this covariance analysis, the determination of the uniform grid to which the individual RBPE observations are to be optimally interpolated can be made. On the average, the network should contain enough grid nodes so that the signal can be resolved approximately twice each scale length. Therefore, the grid sizes chosen are: in time 1 year; in meridional space 5 degrees latitude; and in zonal space 10 degrees longitude.

5. Patterns of BPE variability

The RBPE values used to compute the covariance matrix in the previous section are next interpolated to the regular grid network (i.e., 5 degrees latitude, 10 degrees longitude, 1 year). Also, the RMS error is computed on this grid network. To obtain the interpolate BPE fields themselves, the IRBPE fields should be added back into the annual mean shown in Figure 3. This will not be done here; in fact, the

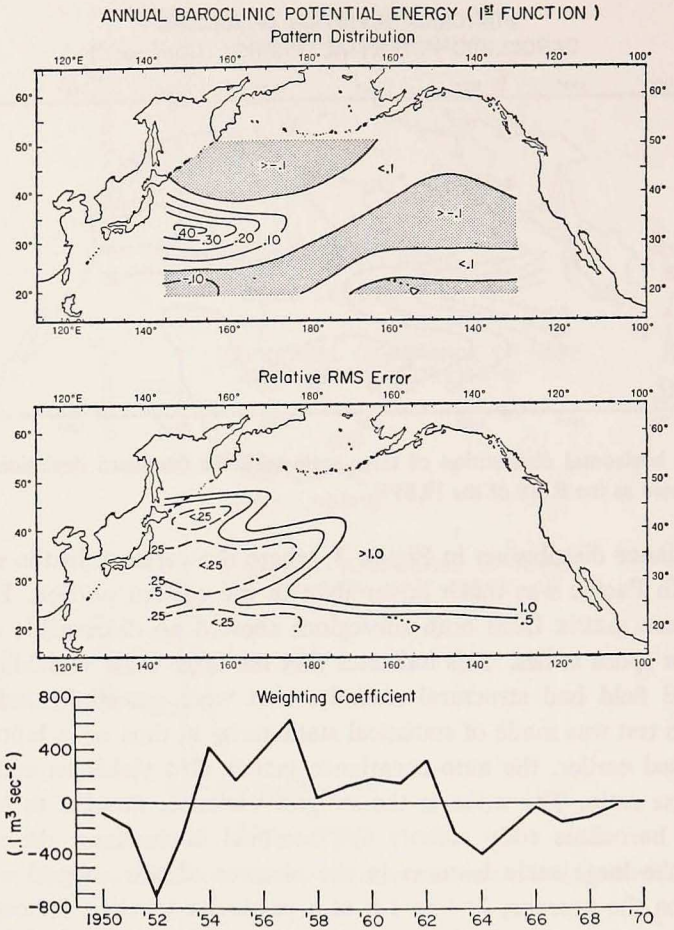

Figure 6. The first empirical pattern, accounting for 47% of the large-scale variance.

21 maps of IRBPE will not be shown either. Rather the characteristic patterns of IRBPE variability are shown, computed from the method of empirical orthogonal function analysis (Lorenz, 1959). A thorough study of these characteristic patterns of IRBPE and their associated error distributions is then given.

Proceeding with the discussion of results, the RBPE individual data are optimally interpolated to form IRBPE in the grid network (i.e., 5 degrees latitude, 10 degrees longitude, 1 year). The spatial distribution of the RMS of the resulting fields of IRBPE is given in Figure 5, where the largest values existed along the axis of the North Pacific Current, being two or three times larger west of 180 longitude than east. Note that the distribution of large-scale standard deviation was very similar to the overall standard deviation shown in Figure 3. Over most of the region, the large scale standard deviation is about half that of the total standard deviation

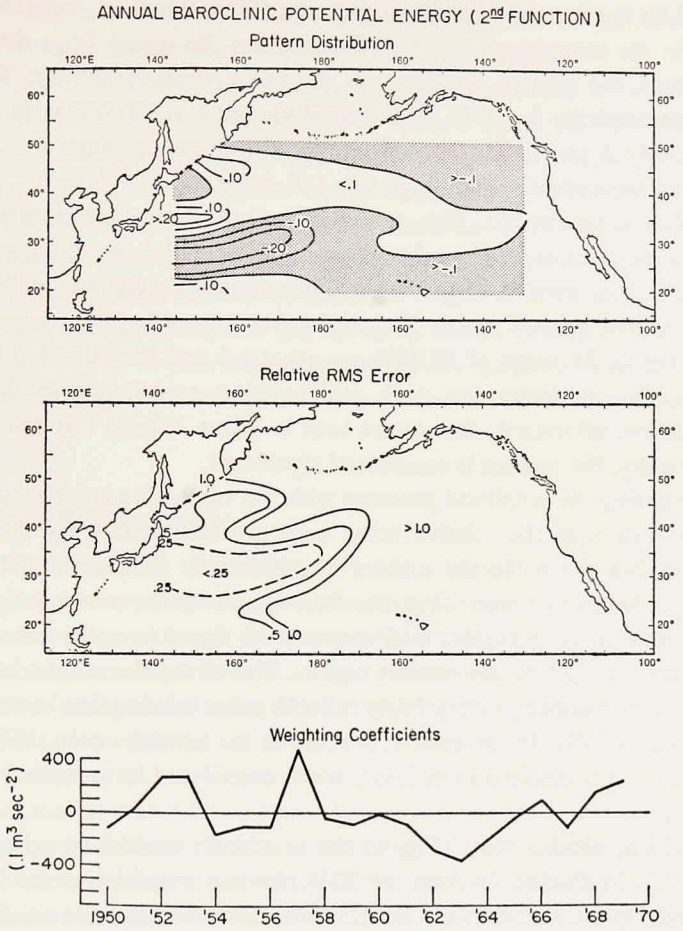

Figure 7. The second empirical pattern, accounting for 20% of the large-scale variance.

shown in Figure 3, which is consistent with the signal to noise ratio of unity. However, in the Western North Pacific along the North Pacific Current, the large scale standard deviation is larger. This arises from the suppression of bias inherent in the optimum interpolation methodology used to estimate the large scale standard deviation, absent in the bulk computation of the total standard deviation. Therefore, the total standard deviation in Figure 3 is underestimated in this region due to the lack of data independence arising from the "burst" mode of sampling.

The technique of empirical orthogonal function analysis is next applied to the 21 maps of IRBPE. What this does is to express the time/space variability displayed in these maps in terms of a superposition each year of stationary patterns, which are the natural empirical modes of the basin. The application of this method yields satisfying results; i.e., nearly 70% of the total large-scale variance in Figure 5 can

be explained by the first two empirical patterns (Figs. 6 and 7), indicating not only the success in the mapping technique of extracting the signal from the noise, but, more important, the relative simplicity of the space/time variability. The first empirical pattern accounts for 47% of the total variance in IRBPE with a time scale of approximately 3 years. The second empirical pattern accounts for 20% of the variance with a time scale of approximately 1½ years.

In each of these figures (i.e., Figs. 6 and 7) both the stationary empirical patterns, $G(x, y)$, and the time sequences of their weighting coefficients $A(t)$ are shown, in addition to a spatial pattern of the error. To compute an error map for these empirical patterns, the squared errors [i.e., E^2 in (3.3)] at each 5×10 degree grid location in the original 21 maps of IRBPE are averaged and then divided by that portion of large-scale variance that each grid location contributes to the particular empirical pattern; afterward, the square root is taken. Where this relative error is smaller than unity, the pattern is considered significant.

Upon comparing the empirical patterns with the respective error maps in Figures 6 and 7, the values in the relative error map are less than unity in the western North Pacific, but not so in the eastern North Pacific (i.e., east of 180W). This situation arises for two reasons: first, the data density in the western region is much higher than in the eastern region; and, second, the signal to noise ratio is higher in the western region than in the eastern region. Therefore, the empirical patterns in the western interior ocean portray fairly reliable point information about the space/time variability in BPE. In the eastern portion of the interior ocean, this is not true; however, the pattern configuration itself, when considered in its entirety, may have some significance.

In the first empirical pattern (Fig. 6) the maximum variability existed along the axis of the North Pacific Current at 33N, in the transition zone between the Kuroshio and Oyashio extensions near 150W. Downstream a meander could be found in the otherwise quasi-zonal North Pacific Current. This has the effect of making the variability in the North Pacific Current in the west out of phase with that in the east. Near the center of the Subtropical Gyre at 20N and Subarctic gyre at 45N in the western North Pacific, the variability was in phase; however, because the former is anticyclonic and the latter cyclonic, the strengths of the two gyres were out of phase.

In the second empirical pattern (Figure 7) a strong maximum in variability did not exist, as it did in the first empirical pattern; rather a number of secondary maxima can be found. Those in the northern and southern secondary gyres that make up the totality of the Subtropical Gyre were in phase. This makes the two secondary gyres appear to have expanded and contracted in the meridional direction in phase with one another. Also the Subtropical and the Subarctic gyres in the western North Pacific had strengths that fluctuated out of phase with one another, similar to the first empirical pattern. In contrast, the strength of the Subtropical

Gyre in the western North Pacific and the southern portion of the Alaskan Gyre in the eastern North Pacific appear to have fluctuated in phase.

In each of these empirical patterns the maximum variability is found in the western North Pacific, associated with the more intense mean current structure found there. This is in contrast to the empirical pattern produced for sea surface temperature by Davis (1976), where the low order variability is found to be maximum in the interior portion of the North Pacific. On the other hand, this latter comparison may not be proper since the present study uses yearly mean data, while Davis is using monthly mean data. On the basis of the work by White and Walker (1974) concerning the vertical structure of annual mean sea surface temperature, it can be expected that the year-to-year variability of annual mean sea surface temperature would have variability that resembles that found in the BPE. However, this remains to be seen.

6. Magnitude of BPE variability

Rather than investigate the magnitude of the large-scale variability in IRBPE directly, an indirect approach is used; i.e., investigating the changes in the zonal baroclinic transport per unit width associated with the empirical pattern variability discussed earlier. The zonal baroclinic transport from 25-45N across 160E is investigated, establishing the magnitude of change in both the Kuroshio and Oyashio extensions. This also allows a comparison with other transport computations from around the North Pacific.

The meridional profile of the zonal baroclinic transport per unit width along 160E is displayed in Figure 8. The climatological mean is shown, as well as the variability about that mean associated with first and second empirical patterns. The zonal baroclinic transport is computed according to (2.2) from the meridional gradient of IRBPE. In the upper panel of the figure, the climatological mean zonal transport of the Kuroshio extension at 30N and the Oyashio extension at 40N are displayed, with the transition region in-between. The error bars represent the standard error; the right-hand scale indicates the vertically averaged zonal speed. Therefore, relative to 500 db, the Kuroshio and Oyashio extension had a vertically averaged zonal speed of 2-3 cm/sec. The overall baroclinic transport across this section was approximately 18 Sv.

Farther to the east, at 135E, the climatological mean baroclinic transport of the Subtropical Gyre was found by White (1975) to be approximately 20 Sv (0/500 db). Yet, at 160E the Kuroshio extension had a transport value of about 11 Sv. Therefore, approximately 8 Sv had passed south and out of the Kuroshio extension, probably as part of an intense recirculation associated with the Subtropical Gyre at 30N, 150E (see Fig. 3).

In subsequent panels of Figure 8, the climatological mean profile is repeated,

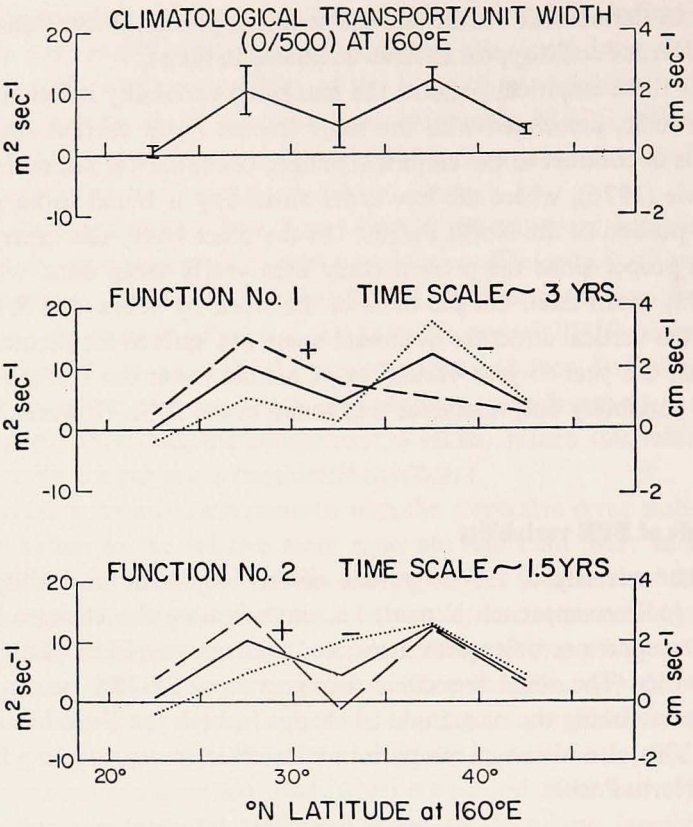

Figure 8. The climatological mean meridional profile of zonal baroclinic transport along 160E from 25-45N. Also shown is the variability (i.e., standard deviation) about this mean profile attributed to the first and second empirical patterns.

together with the variability in that profile associated with the first and second empirical patterns. The envelope drawn represents the plus/minus standard deviation of the variability about the mean zonal flow.

From the first pattern (middle panel, Fig. 8), the strength of the Kuroshio extension was out of phase with that of the Oyashio extension, consistent with remarks made earlier. The magnitude of variability in zonal speed was nearly ±50% of the climatological mean. On the other hand, the change in the meridionally average transport was nearly zero, i.e., the increase in strength of the Subtropical Gyre was offset by a decrease in the Subarctic Gyre, with the converse also true.

With regard to the second pattern (lower panel, Fig. 8) the strength of the Kuroshio extension fluctuated ±50% about the climatological mean, with virtually no change in the Oyashio extension. However, as with the first empirical pattern, the change in the meridionally averaged transport was again near zero; i.e., the

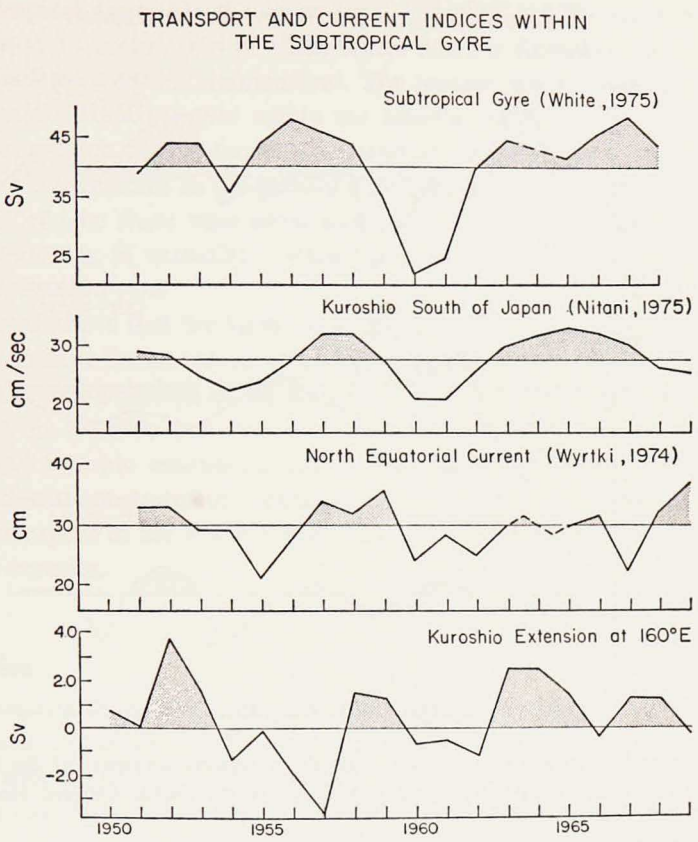

Figure 9. Comparison of the time sequence of the baroclinic transport of the Kuroshio extention at 160E (1 Sv = 10^6 m^3 sec^{-1}) with other transport and current indices around the Subtropical Gyre.

increase in transport of the Kuroshio extension was offset by a decrease in the transition region at 35N, with the converse also true.

The changes in baroclinic transport noted in Figure 8 are next compared with other studies where time sequences of the large-scale variability have been produced. In Figure 9 are three such time sequences from various locations around the Subtropical Gyre, which are the only time sequences of which the author is aware. The first is an index of the baroclinic transport of the Subtropical Gyre (White, 1975) computed from the difference in BPE between ocean weather station *T* (29N, 135E) and a repeated CalCOFI station at 30N, 120W. The second is an index of the surface current in the Kuroshio (Nitani, 1975) computed from hydrographic data taken south of Japan. The third is an index in the strength of the North Equatorial Current (Wyrtki, 1974) taken as the difference in sea level across the current. Upon inspection of these three time sequences, similarity in phase existed, with a correla-

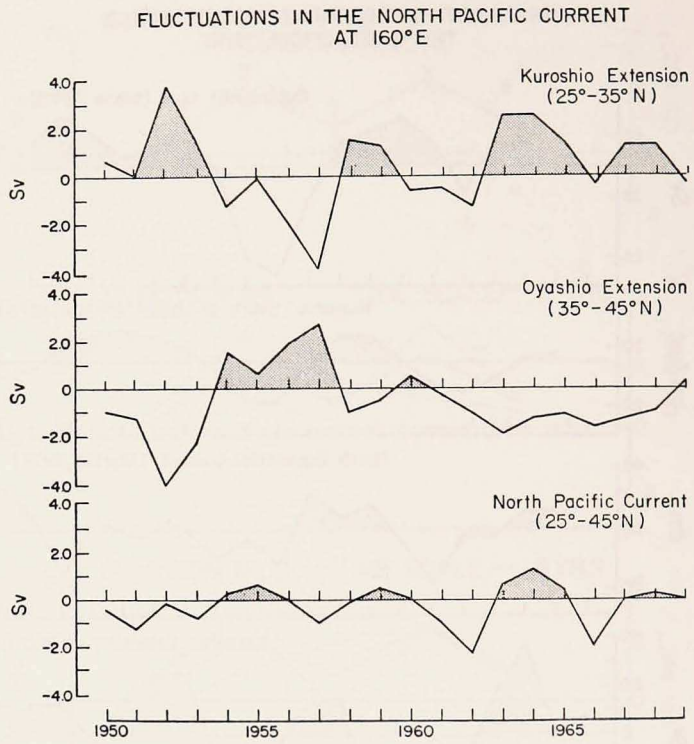

Figure 10. Comparison of the time sequences of the baroclinic transport of the Kuroshio extension at 160E with that of the Oyashio and the North Pacific Current along the same meridian.

tion time scale of approximately 1-2 years. Moreover, the maximum range of variability about the climatological mean in each case was about the same, approximately ±25%.

For comparison with these three time sequences, the variability in the zonal transport of the Kuroshio extension from 25-35N at 160E is shown, computed from the first two empirical patterns. This time sequence visually correlates with the other three; any quantitative correlation will require many more years of accumulated data. Better phase agreement between these time sequences is lacking for two reasons: first, only data associated with the first two empirical patterns were used in the computation of the Kuroshio extension index; and second, the mean general circulation is so complicated that it is difficult to obtain a "precise" measure of its strength at any one location. For example, Nitani's (1975) index measures the baroclinic transport associated with only that portion of the Kuroshio that runs west of the Ryukyu islands, ignoring that portion that runs east of this island chain. This is in contrast to White's (1975) index, which measures the transport of both parts of the Kuroshio by measuring the transport of the northern secondary gyre

of the Subtropical Gyre. On the other hand, Wyrtki's (1975) index measures the North Equatorial Current, part of which enters into the Kuroshio and part of which goes into the Subtropical Countercurrent. The present index measures that portion of the Kuroshio extension that enters the interior as the North Pacific Current, ignoring that portion that recirculates as part of the northern secondary gyre. In light of these complexities in the general circulation, the fact that any phase agreement exists between these time sequences is remarkable, and is testament to the internal consistency of variability within the entire fabric of the Subtropical Gyre in the North Pacific.

It was noted above that the Subtropical and Subarctic gyres in the western North Pacific tend to have fluctuated out of phase with one another. To more fully develop this result, the time sequence of the Kuroshio extension transport is plotted together with that of the Oyashio and their sum, the North Pacific Current (Fig. 10). The Kuroshio and Oyashio extensions tend to have fluctuated out of phase with one another and with comparable magnitudes. Hence, the variability in the overall baroclinic transport of the North Pacific Current was much smaller than in the two component currents.

7. Conclusion

The objectives of this study are to establish the large-scale space/time variability in the baroclinic structure of the interior North Pacific from 1950-1970. To attain these goals with the limited hydrographic data available requires improved methodology. A method of analysis is chosen that both separates the signal from the noise and synthesizes the results in a way that can most easily be communicated to others. Essentially, the methodology is the same as that used by meteorologists in the study of global-scale time-dependent atmospheric phenomena.

Briefly, the method is as follows. The baroclinic potential energy (BPE) is used as a bulk measure of the baroclinic structure of the upper ocean. From the available hydrographic data, the long term mean distribution of BPE is computed from which the BPE values at each hydrographic station are subtracted, yielding a set of residual BPE (RBPE) values. Doing a complete structural analysis upon the time/space distribution of the RBPE field, a dominant signal is found with time and space scales of years and thousands of kilometers, respectively. This means that the resolution required to detect this dominant variability is one year in time, five-hundred km in the meridional direction, and one-thousand km in the zonal direction. The information of this statistical structure is next utilized in an optimum interpolation technique to place the RBPE data on a uniform grid of this resolution. This technique interpolates the irregularly distributed RBPE data to a uniform grid by minimizing the expected interpolation error in a least squares sense. Twenty-one annual maps of optimally interpolated RBPE (IRBPE) from 1950-1970 are con-

structed, together with the RMS error maps. To synthesize the information contained in these maps, the method of empirical orthogonal function analysis is employed. Thus, the information contained in these twenty-one maps of IRBPE is reduced to two recurring empirical patterns which, when added and weighted appropriately, account for 70% of the total interannual variance contained in the original IRBPE maps. It is upon these empirical patterns and the time sequence of their weighting functions that study is concentrated.

From autocorrelation analysis the first empirical pattern of IRBPE variability has a correlation time scale of approximately 3 years, the second a time scale of approximately 1½ years. The first pattern show maximum variability in the western North Pacific at 33N in the transition zone between the Kuroshio and Oyashio extensions, such that the fluctuations in the baroclinic transport of these latter currents were out of phase with one another, as was also true of their respective gyres. The second empirical pattern show variability maxima in the center of the Subtropical Gyre, such that fluctuations in the baroclinic transport of the Kuroshio extension were much larger and out of phase with those of the Oyashio extension.

From the reconstructed time sequence from 1950-1970 of the baroclinic transport of the Kuroshio extension, this transport varied by ±50% of climatological mean and fluctuated nearly in phase with the Kuroshio south of Japan (Nitani, 1975), the large-scale bulk transport of the Subtropical Gyre (White, 1975), and the North Equatorial Current (Wyrtki, 1974). Therefore, the baroclinic transport of the component currents over the entire Subtropical Gyre tends to have fluctuated in unison and in concert with the changes in the large-scale baroclinic structure of the Subtropical Gyre. On the other hand, these currents tend to have been out of phase with the strength of the Subarctic Gyre. As such, the net transport of the North Pacific Current fluctuated much less than its component currents.

As an extension of these efforts, it would be worthwhile to investigate more closely the large-scale variability of the regions marginal to the study, i.e., the tropical and equatorial regions, and the eastern and western boundary current regions. These regions need special consideration because of their larger gradients; on the other hand, the eastern and western boundary regions have a data density that is two orders of magnitude larger than is found in the interior. The tropical and equatorial regions probably have a paucity of data that may make this kind of study impossible for a number of years.

Acknowledgments. The author extends his appreciation to Anthony Tubbs who, as programmer, guided these data through the routines of optimum interpolation and empirical orthogonal function analysis with alacrity. Appreciation is extended to Robert Bernstein and Russ Davis who together developed the optimum interpolation routines at Scripps Institution, and to John Faust who developed the empirical orthogonal function routines. Appreciation is also extended to Ted Walker who, as assistant programmer, implemented many of the secondary analyses in this study.

This research was sponsored by the Office of Naval Research under ONR Contract N000-14069-A-0200-6043, and by the University of California, San Diego, Scripps Institution of Oceanography through NORPAX.

REFERENCES

Alaka, M. A. and R. C. Elvander. 1972. Optimum interpolation from observations of mixed quality. Monthly Weather Review, *100,* 612–624.

Bernstein, R. L. and W. B. White. 1974. Time and length scales of baroclinic eddies in the central North Pacific Ocean. J. Phys. Oceanog., *4,* 613–624.

Dantzler, L. 1976. Geographical variations in intensity of the North Atlantic and North Pacific oceanic eddy fields. Deep-Sea Res., *23,* 783–794.

Davis, R. E. 1976. Predictability of sea surface temperature and sea level pressure anomalies over the North Pacific Ocean. J. Phys. Oceanog., *6,* 249–266.

Gandin, L. S. 1963. Objective Analysis of Meteorological Fields. Gidrometeorologicheskoe Izdatel'stvo, Leningrad, USSR, 286 pp.

Lorenz, E. N. 1959. Empirical orthogonal functions and statistical weather prediction. Report No. 1, Statistical Forecasting Project, Dept. Meteor. M.I.T.

McWilliams, J. 1976. Maps from the Mid-Ocean Dynamics Experiment: Part II. Potential vorticity and its conservation. J. Phys. Oceanog., *6,* 828–846.

Meyers, G. 1975. Seasonal variation in the transport of the Pacific North Equatorial Current relative to the wind field. J. Phys. Oceanog., *5,* 442–449.

Namias, J. 1972. Space scales of sea surface temperature patterns and their causes. Fish. Bull., *70,* 611–617.

Nitani, H. 1975. Variation of the Kuroshio south of Japan. J. Oceanog. Soc. Japan, *31,* 16–35.

NORPAC Atlas. 1960. Oceanic observations of the Pacific: 1955. Prepared by the NORPAC Committee, University of California Press, 123 maps.

Reid, J. 1973. Northwest Pacific Ocean waters in winter. John Hopkins Oceanographic Studies *5,* 96 pp.

Reid, J. and R. Arthur. 1975. Interpretation of maps of geopotential anomaly for the deep Pacific Ocean. J. Mar. Res., *33,* 37–52.

White, W. B. 1975. Secular variability in the large-scale baroclinic transport of the North Pacific from 1950-1970. J. Mar. Res., *33,* 144–155.

—— 1977. Annual forcing of baroclinic long waves in the tropical North Pacific Ocean. J. Phys. Oceanog., *7,* 50–61.

White, W. B. and A. E. Walker. 1974. Time and depth scales of anomalous subsurface temperature at ocean weather stations P, N, and V in the North Pacific. J. Geophys. Res., *79,* 4517–4522.

White, W. B. and R. L. Bernstein. 1977. Statistical analysis leading to the design of an optimum oceanographic network in the upper waters of the mid-latitude North Pacific Ocean. J. Phys. Oceanog. (in review).

Wyrtki, K. 1967. Spectrum of ocean turbulence over distances between 40 and 1000 km. Deutche Hydrographische Zeitshrift, *20,* 176–196.

—— 1974. Equatorial currents in the Pacific 1950-1970 and their relation to the winds. J. Phys. Oceanog., *4,* 372–380.

—— 1975. Fluctuations of the dynamic topography in the Pacific Ocean. J. Phys. Oceanog., *5,* 450–459.

Yoshida, K. and T. Kidokoro. 1967. A subtropical countercurrent (II)—a prediction of eastward flows at lower subtropical latitudes. J. Oceanog. Soc. Japan, *23,* 231–246.

Received: *16 June, 1976;* revised: *10 March, 1977.*